IMPACT OF CeO_2 NANOPARTICLES AND SODIUM CHLORIDE (NaCl) ON SOIL WATER POTENTIAL AND DISTRIBUTION

A Thesis

by

BRITTANY L. HALLMARK

Submitted to the Office of Graduate and Professional Studies of
Texas A&M University
in partial fulfillment of the requirements for the degree of

MASTER OF SCIENCE

Chair of Committee,	Rabi H. Mohtar
Co-Chair of Committee,	Xingmao Ma
Committee Members,	Amjad T. Assi
	Paul Schwab
Head of Department,	Robin Autenrieth

August 2017

Major Subject: Civil Engineering

ABSTRACT

Engineered nanoparticles are more and more being released into the environment even though not much is known about how these NPs will behave in the soil environment. CeO_2 NPs have a wide range of applications, and therefore have a high likelihood of environmental release. Additionally, salinity is becoming an increasingly more important issue as freshwater supply is dwindling and saline soils are increasing.

The goal of this study was to investigate how CeO_2 nanoparticles (NPs), sodium chloride (NaCl), and their interaction impact soil water potential and distribution. Three CeO_2 NP concentrations and two NaCl concentrations were chosen to determine the impact and interaction of these two stressors on the soil-water environment by using the Typosoil™ to measure the water retention curve (WRC) and soil shrinkage curve (ShC). These two soil-water characteristics curves can be used to determine the potential and distribution of the soil-water environment.

The results showed there was not enough conclusive data to determine the impact of NaCl and the interaction of NaCl and CeO_2 NPs on the soil. However, under no salt conditions, increasing CeO_2 NPs concentration increased the potential of the microdomains of the soil, making it more difficult to remove water from this area. Overall, the total water storage didn't change, but the distribution of water shifted towards the macrodomain. In conclusion, the results demonstrated that the CeO2 nanoparticles do have an effect on soil properties.

ACKNOWLEDGEMENTS

I would like to thank my committee chair, Dr. Mohtar, co-chair, Dr. Ma, and members, Dr. Schwab and Dr. Assi, for their help and support throughout the course of this research.

I would also like to thank my friends and colleagues, especially Sonja Loy, who was of great assistance to me in the lab. Thanks also goes to the department faculty and staff in Biological and Agricultural Engineering and Civil Engineering. They all made my experience at Texas A&M an enjoyable one.

CONTRIBUTORS AND FUNDING SOURCES

Contributors

This work was supported by a thesis committee consisting of Professor Mohtar (chair), Professor Ma (co-chair), and Professor Assi (Civil Engineering) and Professor Schwab (Soil and Crop Sciences).

All work for the thesis was completed by the student, under the advisement of Dr. Rabi H. Mohtar of the Departments of Civil Engineering and Biological and Agricultural Engineering and Dr. Amjad Assi of the Department of Biological and Agricultural Engineering.

Funding Sources

Graduate study was supported by a fellowship from Texas A&M University.

TABLE OF CONTENTS

Page

Page

LIST OF FIGURES

Page

LIST OF TABLES

Page

1. INTRODUCTION

1.1 Introduction to Problem

Nanotechnology is an emerging field in science and technology, which has led to large scale production of engineered nanoparticles (ENPs). ENPs have a unique set of properties that are different from the bulk material, such as increased specific surface area [2]. These properties make ENPs useful in a wide variety of applications, including medicines, catalysts, cosmetics, pharmaceuticals, sporting goods and microelectronics [3-6]. Industries involved in the synthesis and application of ENPs are currently a largely growing industry. They are expected to reach $3 trillion by 2020 [7]. Since ENPs have different properties than the bulk material, their behavior and interaction with surroundings are expected to be different, such as the increased mobility [8]. The increased use of ENPs has raised concerns about their environmental impacts. The two major pathways for environmental exposure from ENPs is water irrigation and biosolids land application [1].

Cerium is one of the most abundant rare earth metals, and cerium oxide nanoparticles (CeO_2 NPs) are part of the rare earth metal oxide nanoparticle group. This NP group is industrially and commercially important for paint coatings, polishing powder, microelectronics, and catalysts [5]. It is estimated that between 100 and 1000 tonnes of CeO_2 NPs are produced every year [1]. One of the unique properties of CeO_2 NPs is the UV-radiation absorption capacity[9]. This makes them especially useful for sunscreen and cosmetic products. Another major application of CeO_2 NPs is as a fuel additive to reduce pollutant release and increase the combustion efficiency [9]. These

broad applications make it highly likely that CeO_2 NPs will gradually build up in the environment and therefore, their environmental consequences need to be investigated.

A growing world population requires an increase in water resources. However, there is a growing decrease in freshwater supply[1, 10], and it is unevenly distributed across the globe[10]. Agriculture is the largest consumer of water globally[10]. New water sources are necessary to keep up with the demand: desalinization of seawater and brackish water, rainwater harvesting, and the use of saline water[10]. Saline water sources include wastewater, agricultural drainage water, and saline groundwater[10]. These sources could introduce varying amounts of salt into the soil environment. There is also a rising amount of soil that is classified as salt affected or saline[11]. A soil is considered saline when the water extracted from the saturated soil has approximately a concentration of around 40 mM of dissolved salts. The most common cations in soil are Ca^{2+}, Mg^{2+}, K^{+}, and Na^{+}, and the anions are Cl^{-}, So_4^{2+}, HCO_3^{-}, and NO_3^{-} [11, 12]. 800 million hectares of land globally are salt affected[13]. This corresponds to 6% of the total arable land and 20% of irrigated farmland. Soil can become saline through natural causes: accumulation of salt from rain and wind deposition[12], or agricultural practices: application of soluble fertilizers and soil amendments, poor quality irrigation water, and land clearing [11, 12]. Climate change has increased soil desertification, which then can cause soil salinization [14].

1.2 Objectives

The objective of this research is to study and understand the impact of

(a) cerium oxide nanoparticles (CeO_2 NPs),

(b) sodium chloride (NaCl),

(c) the intersection of CeO_2 NPs and NaCl, and

(d) application method

on the soil-water parameters, including potential, storage, and distributionwithin the soil profile.

1.3 Hypotheses

The expected outcomes of this study include the following:

(a) CeO_2 NPs will interact with clay particles in the microdomain The expected outcome (positive or negative) is unclear, as per the interaction of CeO_2 NPs with plants (below in section 2.1)

(b) NaCl should reduce the water storage and retention properties of soil.

(c) CeO_2 NPs could counteract some of the negative effects of NaCl on soil-water characteristics to some degree.

(d) The trends between the two application methods should be similar, but due to the distribution of CeO_2 within the soil, it is possible that the impact of CeO_2 NP would be more pronounced in the mixing method.

2. BACKGROUND

2.1 CeO_2-NPs and Plants

The interaction of CeO_2-NPs and plants has been extensively studied. The results are mixed as to whether CeO_2-NPs is beneficial or harmful to plants. The root elongation of lettuce was inhibited after exposure to 2000 mg/L CeO_2-NPs solution for 5 days. Tomato, radish, rape, wheat, cucumber, and cabbage showed no differences under the same conditions [2]. Some studies have showed that low concentrations of CeO_2-NPs have negligible or slightly beneficial results on plants, while higher concentrations are detrimental. Wang 2012 [9] showed irrigating with a 10 mg/L CeO_2-NPs solution improved tomato growth and yield. Lopez-Moreno 2010 [15]showed that concentrations above 2000 mg/L CeO_2-NPs were damaging to soybean growth, but lower concentrations had no impact.

Rossi 2016 [1] examined the interaction of CeO_2-NPs and salt on canola plants. This study demonstrated that salt-stressed plants treated with CeO_2-NPs did better than plants without, although the CeO_2-NPs were not fully able to counteract the negative consequences of the salt treatment. Furthermore, plants treated with CeO_2-NPs (both with and without salt stress) had increased levels of chlorophyll, better light use efficiency, and higher proline content.

The impact of CeO_2-NPs on plants is well characterized. The impact depends on the plant species, exposure concentration, exposure duration, and plant growth conditions [2, 6, 9, 16, 17].

2.2 NPs and Soil

The fate and behavior of nanoparticles in soils has been studied frequently but very few studies examine the impact of the nanoparticles on the soil. There are five soil-forming factors that determine soil structure and properties over a geological time scale: geological/parent materials, climate, topography, biota, and time. Yaron argues that anthropogenic activity could be a sixth factor [18]. Anthropogenic behaviors can cause irreversible physical, mechanical, and chemical transformations to the soil structure and properties. To be irreversible, these changes need to be long-term, stable, and persistent to the soil matrix, and resistant to remediation and natural attenuation [18]. Furthermore, the impact of anthropogenic activity occurs on a much shorter time scale than the five natural soil-forming factors. The addition of engineered nanomaterials (ENMs) is one anthropogenic behavior that can change the soil. Although ENMs are added to the soil in small amounts, they are oftentimes retained in the soil; therefore, the amount of ENMs present in soil increases over time. The authors of Yaron et. al. 2016 review several publications that examine the impact of nanoparticles on soil properties [18].

Once introduced into the soil environment, there are several pathways for the ENMs to take. They can move through the soil channels or move into the soil pore space to interact with clay particles and organic matter or form aggregates on soil surfaces that can stay in the soil matrix [18]. Westerhoff and Nowack 2013[19] showed that ENMs have similar behavior to chemical contaminants in soil. As such, there are two possible interaction consequences: the ENMS can be affected by the soil or the ENMs can affect the soil properties.

Mogyorosi 2003 [20] showed that TiO_2 NPs formed heteroaggregates with clay particles. These heteroaggregates bind the TiO_2 NP to the clay surfaces [20]. The TiO_2 heteroaggregates showed a change in the clay matrix of montmorillonite by a 1.20 to 3.00 nm clay basal spacing increase. Zhou 2012 [21] showed that the heteroaggregation of TiO_2 ENMs is dependent on pH, ionic strength, and solution composition. The heteroaggregates of ENMs and clay particles can form larger aggregates. This aggregates can interact with multiple clay particles to form a connection between soil surfaces.

Ben-Moshe [22] showed that NPs have an impact on the microscopic properties of the soil. They showed that soil exposed to CuO NPs under strong oxidizing conditions had a different organic matter composition than soil without CuO NPs. In the same study, CuO and iron oxide nanoparticles changed the soil morphology by ENM deposition. Wang 2014 [23] found similar results when Ag coated PVP aggregates were retained on the surface of goethite. Cornelis 2014 [24] demonstrated that ENMs caused a change in the soil isoelectric point. These studies show that ENMs can have an impact on soil properties.

One theory about ENM deposition on soils is that ENMs attach to soil surfaces in the pores, which can change the behavior of water in the pores. This is called pore clogging, and it is demonstrated by Ng and Coo 2014[25]. CuO ENMs on kaolin clay decreased the hydraulic conductivity by 45% and decreased pore size by 20%. Tellam 2011 [26] showed that metal oxides caused pore clogging in sandstone, and Dunphy-Guzman 2006 [27] showed that TiO2 ENMs aggregates caused pore clogging. Dunphy-Guzman 2006 [27] also found an increase in the water content due to the presence of TiO2 aggregates.

A few select studies have demonstrated the impacts of ENMs on soil properties, proving that anthropogenic activity does change the natural soil. However, this interaction is not well studied and further experimentation is needed.

2.3 Water Holding Capacity

Water holding capacity (WHC) of a soil is the amount of moisture stored in the soil. This is the water that remains in the soil as determined by the capillary action of the soil. This occurs when the soil-water adhesive forces exceed the water-gravity forces [28]. At this point, the water remains in the soil rather than being lost to gravitation water flow [29].Water that is drained from the soil by gravitational forces is the gravitational water. The upper limit of WHC is field capacity, or the maximum available water, and the lower limit is permanent wilting point (PWP) [30]. At the permanent wilting point, all that remains in the soil is residual water [28]. WHC is extremely dependent on pore size, pore quantity, soil texture, soil structure, and organic matter in soil [29-32].

The water available to plants is typically considered to be the same as the WHC [31]. The field capacity is the maximum available water, and at the permanent wilting point, plants can no longer extract water from the soil. However, plant available water can be broken down into the location of the water in the soil. Another concept of WHC is the readily available WHC. This concept states that plants can extract water from larger pores easier than smaller pore (micropores) [30]. This information can be very useful because understanding the WHC of a soil is important to soil-water management. It helps in determining what crops to grow, how many, when and how much to irrigate, and how much fertilizer to use [30, 31].

There are many methods to determine water holding capacity of a soil. The most common are the Food and Agricultural Organization of the United Nations estimates,

pressure plate, and pedotransfer functions [30, 33]. The method used in this study will be the soil shrinkage curve using the TypoSoil.

2.4 TypoSoil

In order to determine the hydro-structural parameters and the soil-water storage and interaction, Assi 2014 and Braudeau 2014 [34, 35] link the soil shrinkage curve (ShC) and the water retention curve (WRC). This is performed through the use of the Typosoil^{TM}, an apparatus that continuously and simultaneously measures the water, content, volume, and retention of the soil for up to 8 soil cores at once. Each core contains 100 cm^3 of soil, and the height, diameter, mass, and pressure is measured for each core every 8 minutes. The continuous and simultaneous measurements allow for the measurement of the data pairs under similar conditions and the same water contents. This provides the data necessary for the determination of inflection points and transition zones that characterize the soil aggregate organization and the determination of hydro-structural parameters. This data can then be fitted to thermodynamic-based equations to model the shrinkage curve (ShC) and the water retention curve (WRC) and estimate the hydro-structural parameters [34-38].

The foundation of the theory of the TypoSoil is based on the pedostructure and structural representative elementary volume (SREV) concepts. Pedostructure defines and describes the soil structure as primary peds [35]. Primary peds are the smallest peds in soil [39]. Each primary ped is an aggregate of several primary particles, as determined by soil type. Primary peds are the first level of soil organization, and they are capable of forming larger aggregates (Figure 1). The assembly and formation of aggregates from these primary peds into a soil structure is the pedostructure concept. The classic REV theory uses the volume of the soil sample as a reference point. This is

an issue because the volume does not stay constant. As such, the REV concept ignores internal organization of the soil structure (pedostructure) and cannot define and describe the soil-water physical interactions The SREV is a closed thermodynamic system based on the dry mass of the soil sample, not the volume of the solid phase. The dry mass stays constant so the SREV is able to use soil-water thermodynamics to describe the pedostructure as two nested and complimentary sub-pore systems: the micro and macro pores. The microdomain is the space within the primary peds, and the macrodomain is the space outside the primary peds. The SREV concept is able to describe and simulate all dynamic processes in the within a pedon through a soil-water thermodynamic standpoint. The use of the pedostructure and SREV concepts with the TypoSoil are able to model and characterize the interaction of the soil structure and soil water dynamics. The variables from the SREV concept that use the dry mass M_s as a reference are characterized by a bar above the variable, such as the specific water content ($\overline{W}$) [34-37, 40].

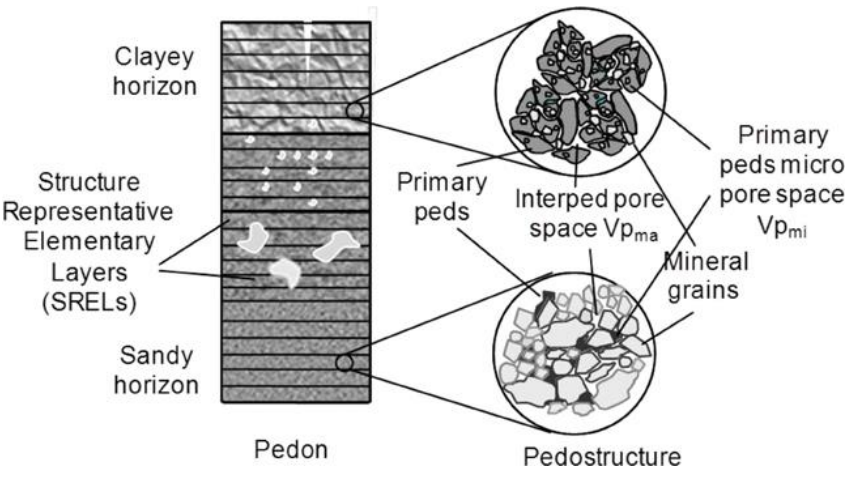

Figure 1: The primary peds and organization of soil, and the interped pore space. Reprinted from [35].

Two important factors that are calculated first from the Typosoil data are the specific volume ($\bar{V}$) and the specific water content ($\bar{W}$). Two main assumptions are made to calculate specific volume and specific water content: (1) isotropic radial shrinkage, and (2) uniform water distribution throughout the sample. Using these assumptions, equations [1] and [2] can be used to calculate specific volume and specific water content respectively. These two equations, along with the internal tension measurements, can be used to create the ShC and WRC.

$$\bar{V} = \frac{\pi d^2 H}{4 M_s} \quad [1]$$

Table 1: Variables for equation [1], their units, and a brief description.

Variable	Units	Description
$\bar{V}$	$\frac{dm^3}{kg_{solid}}$	Specific volume of the soil sample
d	dm	Diameter of the soil core
H	dm	Height of the soil core
M_s	kg_{solid}	Dry mass of the soil core after drying at 105°C for 48 hours

$$\bar{W} = \frac{m - M_s}{M_s} \quad [2]$$

Table 2: Variables for equation [2], their units, and a brief description.

Variable	Units	Description
$\bar{W}$	$\frac{kg_{H_2O}}{kg_{solid}}$	Specific water content of the soil sample
m	kg_{H_2O}	Measured mass of soil sample

2.4.1 Soil Shrinkage Curve and Water Retention Curve

The soil shrinkage curve (ShC) measures specific volume changes, or the void ratio changes, for a soil sample at each water content [34]. Figure 2 shows an example of a shrinkage curve with its' characteristic inflection points. The ShC begins at full saturation, and water content decreases moving from right to left on the ShC. The ShC is comprised of four phases: interpedal, structural, basic, and residual. Interpedal is the first phase on the far right of the curve. Interpedal water (also called gravitational water) is controlled by gravimetric forces, and it drains freely from the soil. The transition from interpedal water to structural water is marked by transition point L. Structural water has a stronger adhesive force with the soil than gravity, so the water can be retained by the soil. This transition point L can also be correlated to the field capacity [25]. Interpedal and structural water is the moisture outside of the primary peds, which is the water in the macrodomain. Moving further along the ShC to the left, the next transition point is M. This marks the point where the water switches from the macrodomain to the microdomain. All the water has drained from the primary peds, and the micropores are fully saturated. This is the beginning of the basic water phase. Water in the basic phase exists inside the primary peds, and the water is controlled by capillary action and

intramolecular activity from surface functional groups [41].The basic water phase is where most of the volume change occurs. The two reasons for the volume change are water loss and the shrinkage of the primary ped. As moisture is removed from the basic phase, the primary peds get smaller to account for this water loss; ergo, the primary peds continue to be full with water even as the water content decreases. The point where air begins to enter the primary peds occurs at transition point N. This marks the transition into the residual water phase. In this phase, the volume of the primary peds stops changing with the loss of water content. Residual water is the moisture that is leftover after accessible water has evaporated, and this is the dry water content of the primary peds where water is no longer accessible. Transition point N corresponds to the permanent wilting point [34, 35]. The shrinkage curve and subsequent phases and transition points will be determined using the TypoSoil.

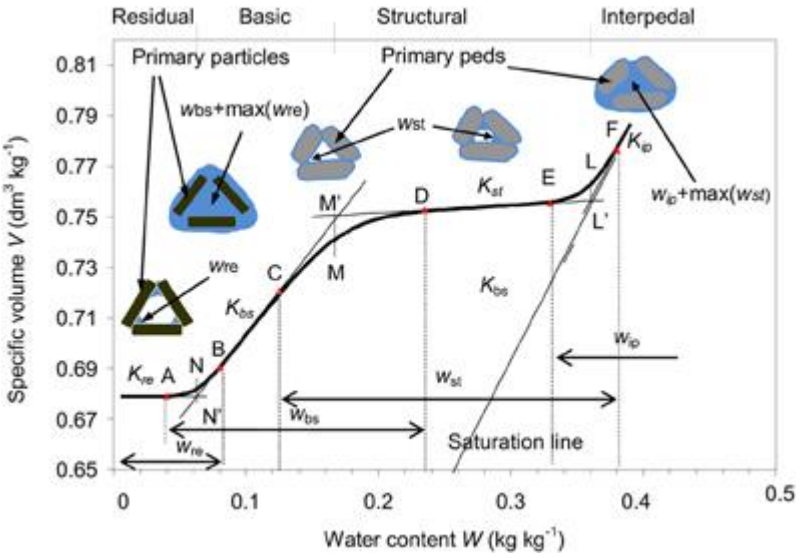

Figure 2: Shrinkage curve (ShC) showing the transition points and water phases. The interpedal and structural water phases are the water in the macrodomain, and the basic and residual water phases are the moisture in the microdomain. Reprinted from [35].

The soil water retention curve is the soil suction at each water content. It measures the soil-water potential [34]. In the TypoSoil, the WRC is created by using a tensiometer, which can only measure tension below 1000 hPa. However, the WRC can be modeled to obtain higher tensions [35].The tensiometer directly measures the pressure of the soil core, given in negative units. This value can be used to calculate the soil-water tension in positive values. The soil-water tension is also known as the soil-water suction, water potential, or water retention (all positive values) [37]. The WRC has two water pools: interpedal and structural, basic, and residual (Figure 3). If it is present, the interpedal water makes up the first part of the curve, and behaves differently than the second part of the curve. The second water pool (thermodynamic) is the structural, basic, and residual phases combined.

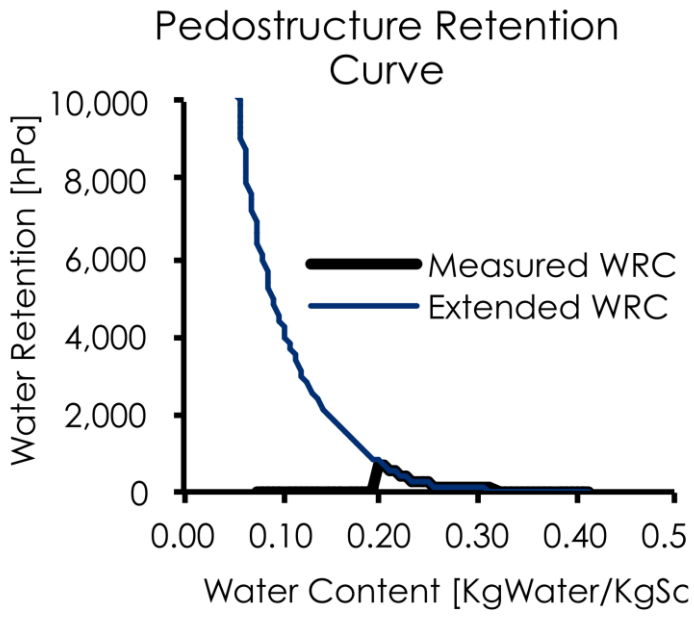

Figure 3: Measured and modeled water retention curve.

2.4.2 State Functions

Once the ShC and WRC have been created from the raw data, state functions can be used to model the curves. There are 12 state variables, also known as the hydro-structural parameters, which are used to create the modeled curves: W_{misat}, W_{masat}, E_{mi}, E_{ma}, V_0, W_N, k_N, K_{bs}, k_{st}, W_L, k_L, and K_{ip}. These parameters and their description and physical units are described in Table 3. It is important to note that the parameters with a bar above the variable means the parameter is divided by the dry mass of the soil sample, while parameters without are simply the raw data. For example, $\overline{W}$ vs W. The former is the specific water content [kg_{H20}/kg_{solid}], and the latter is the water content [kg_{H20}].

Table 3: The 12 state variables (hydro-structural parameters), their units, and a brief description

Parameter	Units	Description
$\boldsymbol{W_{misat}}$	kg_{H_2O}	Water content of micropores at saturation
$\boldsymbol{W_{masat}}$	kg_{H_2O}	Water content of macropores at saturation
$\boldsymbol{\bar{E}_{mi}}$	$\frac{J}{kg_{soil}}$	Potential energy on the surface of the micropores
$\boldsymbol{\bar{E}_{ma}}$	$\frac{J}{kg_{soil}}$	Potential energy on the surface of the macropores
$\boldsymbol{\bar{V}_0}$	$\frac{dm^3}{kg_{soil}}$	Specific volume when there is no observable change in water content
$\boldsymbol{W_N}$	kg_{H_2O}	Water content when primary peds are dry
$\boldsymbol{k_N}$	$\frac{kg_{soil}}{kg_{H_2O}}$	Vertical distance between N and N’
$\boldsymbol{K_{bs}}$	$\boldsymbol{\frac{dm^3}{kg_{H_2O}}}$	The slope of the basic shrinkage phase of the ShC
$\boldsymbol{K_{st}}$	$\frac{dm^3}{kg_{H_2O}}$	The slope of the structural shrinkage phase of the ShC
$\boldsymbol{W_L}$	kg_{H_2O}	Water content when all interpedal water has drained
$\boldsymbol{k_L}$	$\frac{kg_{soil}}{kg_{H_2O}}$	Vertical distance between L and L’

2.4.3 ShC and WRC Derivation Curve

The previously stated hydro-structural parameters are used to create the ShC curve in equation [3]:

$$\bar{V} = \bar{V}_0 + K_{bs}\bar{w}_{bs}^{eq} + K_{st}\bar{w}_{st}^{eq} + K_{ip}\bar{w}_{ip}^{eq} \quad [3]$$

Table 4: Variables for equation [3], the units, and a brief description.

Variable	Units	Description
$\bar{V}$	$\frac{dm^3}{kg_{solid}}$	Specific volume of the soil sample
$\bar{V}_0$	$\frac{dm^3}{kg_{solid}}$	Specific volume of the soil sample at the end of the residual phase
$K_X\ (X = bs, st, ip)$	$\frac{dm^3}{kg_{H_2O}}$	Slope of the basic, structural, or residual ShC phase
$\bar{w}_X^{eq}\ (X = bs, st, ip)$	$\frac{kg_{H_2O}}{kg_{solid}}$	Specific water pools (basic, structural, or interpedal) of the linear shrinkage phase

$\bar{w}_{bs}^{eq}$, $\bar{w}_{st}^{eq}$, $\bar{w}_{ip}^{eq}$ can be defined by equations [4], [5], and [6]:

$$\bar{w}_{bs}^{eq} = \bar{W}_{mi}^{eq} - \bar{W}_{re} = \frac{1}{k_N}\ln\left[1 + \exp\left(k_N\left(\bar{W}_{mi}^{eq} - W_{miN}^{eq}\right)\right)\right] \quad [4]$$

$$\bar{w}_{st}^{eq} = W_{ma}^{eq} = \bar{W} - W_{mi}^{eq} \quad [5]$$

$$\bar{w}_{ip}^{eq} = \frac{1}{k_L}\ln\left[1 + \exp\left(k_L(\bar{W} - \bar{W}_L)\right)\right] \quad [6]$$

Table 5: Variables for equations [4], [5], and [6], the units, and a brief description.

Variable	Units	Description
$k_X\ (X = L, M, N)$	$\frac{kg_{soil}}{kg_{H_2O}}$	Vertical distance between intersection points X and X' on the shrinkage curve (figure 2)
$\bar{W}_{ma}^{eq}$	$\frac{kg_{H_2O}}{kg_{solid}}$	Macropore water content outside the primary peds
$\bar{W}_{mi}^{eq}$	$\frac{kg_{H_2O}}{kg_{solid}}$	Micropore water content
$\bar{W}_{miN}^{eq}$	$\frac{kg_{H_2O}}{kg_{solid}}$	Micropore water content calculated using $\bar{W}_N$ instead of $\bar{W}$ (equation [7])
$\bar{W}$	$\frac{kg_{H_2O}}{kg_{solid}}$	Total pedostructure water content
$\bar{w}_{re}$	$\frac{kg_{H_2O}}{kg_{solid}}$	Specific water pool of the residual phase

$\bar{W}_{mi}^{eq}$ and $\bar{W}_{ma}^{eq}$ can be calculated using equations [7] and [8]. To calculate $\bar{W}_{miN}^{eq}$, use equation [7], and replace $\bar{W}$ with $\bar{W}_N$. Equations [9], [10], and [11] can be used to calculate variables used in equations [7] and [8].

$$\bar{W}_{mi}^{eq}(\bar{W}) = \bar{W} - W_{ma}^{eq} = \frac{\left(\bar{W} + \frac{\bar{E}}{A}\right) + \sqrt{(\bar{W} + \frac{\bar{E}}{A})^2 - (4\frac{\bar{E}_{ma}}{A}\bar{W})}}{2} \quad [7]$$

$$\bar{W}_{ma}^{eq}(\bar{W}) = \frac{\left(\bar{W} - \frac{\bar{E}}{A}\right) - \sqrt{(\bar{W} + \frac{\bar{E}}{A})^2 - (4\frac{\bar{E}_{ma}}{A}\bar{W})}}{2} \quad [8]$$

$$A = \frac{\bar{E}_{ma}}{\bar{W}_{masat}} - \frac{\bar{E}_{mi}}{\bar{W}_{misat}} \quad [9]$$

$$\bar{W}_{sat} = \bar{W}_{masat} + \bar{W}_{misat} \quad [10]$$

$$\bar{E} = \bar{E}_{ma} + \bar{E}_{mi} \quad [11]$$

Table 6: Variables for equations [7], [8], [9], [10], and [11], the units, and a brief description.

Variable	**Units**	**Description**
A	*Constant*	Constant that compares the chemical potentials of the micro and water types at saturation
$\bar{W}_{masat}$	$\frac{kg_{H_2O}}{kg_{solid}}$	Macro water content at saturation
$\bar{W}_{misat}$	$\frac{kg_{H_2O}}{kg_{solid}}$	Micro water content at saturation
$\bar{W}_{sat}$	$\frac{kg_{H_2O}}{kg_{solid}}$	Water content of soil sample at saturation
$\bar{E}_{ma}$	$\frac{J}{kg_{soil}}$	Potential energy of surface charges on outside of primary peds
$\bar{E}_{mi}$	$\frac{J}{kg_{soil}}$	Potential energy of surface charges on inner surfaces of primary peds
$\bar{E}$	$\frac{J}{kg_{soil}}$	Potential energy of surface charge of soil sample

The water retention curve is derived from equation [12]:

$$h^{eq}(\overline{W}) = \begin{cases} h_{mi}(\overline{W}_{mi}^{eq}) = \rho_W \bar{\bar{E}}_{mi}(\frac{1}{\overline{W}_{mi}^{eq}} - \frac{1}{\overline{W}_{misat}}) \\ h_{ma}(\overline{W}_{ma}^{eq}) = \rho_W \bar{\bar{E}}_{ma}(\frac{1}{\overline{W}_{ma}^{eq}} - \frac{1}{\overline{W}_{masat}}) \end{cases} \quad [12]$$

Table 7: Variables for equation [12], the units, and a brief description.

Variable	Units	Description
h^{eq}	dm ≈ kPa	Soil suction at any water content ($\overline{W}$)
h_{mi}	dm ≈ kPa	Soil suction within the primary peds
h_{ma}	dm ≈ kPa	Soil suction outside the primary peds
ρ_W	1 $\frac{kg_{H_2O}}{dm^3}$	Specific density of water (assumed to be 1)

These equations use the raw data from the Typosoil to create the ShC and WRC curve. The specific hydro-structural parameters can then be extracted directly from these curves. In total, there are 15 hydro-structural parameters, but this study will only focus on 5 of them: W_{sat}, W_N, W_{masat}, W_{misat} and E_{mi}.

2.5 Energy Potential of the Surface Charge of Clay Particles in the Micropore (E_{mi})

E_{mi} is one of the 12 state functions used to model the ShC and WRC. As seen from equation [12], E_{mi} is specifically used to model the WRC. E_{mi} is defined as the potential energy of the surface charge from the solid phase (clay particles) inside the

primary peds (micropores). E_{mi} is a result of the surface charge of the clay particles, and can also be described as the quantity of surface charges of clay particles inside primary peds [35] or the total potential energy (positive) relative to a fixed number of surface charges of solid particles inside primary peds [37]. As such, E_{mi} has a direct relationship between the surface charges of the clay particles: a higher E_{mi} is a result of a higher surface charge density. Surface charge has a direct impact on water retention. A higher surface potential will create a more developed electric double layer, which can increase water retention [42]. Tuller 2005 also found that an increase in surface charge density lead to an increase in adsorbed water [43].

2.6 Double Layer Theory

The diffuse double layer theory is used to describe interactions between ions and a charged surface. In the soil-water environment, clay is typically negatively charged. This attracts cations to the surface of the clay particles. The cations closest to the charged surface are bonded directly to the surface by ionic and covalent bonds [43]. These are the ions in the inner Helmholtz plane where no water is present (inner sphere complexes). The outer Helmholtz plane contains hydrated cations (outer sphere complexes). Here, water acts as a bridge between the cation and charged surface. The inner and outer Helmholtz planes make up the Stern layer. Beyond the Stern layer is the diffuse ion layer. The inner and outer sphere complexes that make up the Stern layer counteract some of the negative charge from the clay surface, but there is still a negative charge present. The diffuse ion layer will contain ions to neutralize the leftover charge from the Stern layer. As the cations move farther away from the charged surface and Stern layer, the concentration decreases until the bulk solution is achieved. The double layers between particles can interact, and this determines some clay properties,

such as swelling, plasticity, and water retention, among other aqueous solution processes [41]. The nature of the interaction between the double layers is dependent on the thickness of the double layer, which comes from factors like electrolyte concentration, electrolyte valence, and electric potential.

The electric potential is generated from the surface potential of the clay particles. An increase in the electric potential corresponds to an increase in the diffuse double layer thickness, assuming all other factors are kept constant. As the diffuse double layer increases, the repulsion between clay particles increases and the particles are pushed away from each other [44]. This causes large volume changes in the soil matrix [44]. This can cause swelling of the clay [45].

In a temperature dependence study, Francois 2012 [46] demonstrated that the water retention was dependent on the double layer thickness. A temperature increase lead to a decrease in the double layer thickness and a decrease in water retention. [46]. El-Swaify 1967 [47] also found that increasing the electrolyte concentration (decreasing the double layer) generally led to a decrease in water retention. Additionally, Ca-clays had lower water-holding capacity than Na-clays. Ca-clays have smaller double layer thickness than Na-clays, further supporting that the double layer does impact the water retention of the soil.

3. MATERIALS AND METHODS

3.1 Methods Overview

Soil was collected and ground and sieved to 2 mm after air drying. Then a metal cylinder of 5 cm height by 5 cm diameter coated with a light layer of petroleum jelly on the inside was placed in a shallow dish filled with water. Soil was slowly and evenly added to the metal cylinder. The soil was allowed to become fully saturated by capillary wetting before the next layer was added. Once the metal cylinders were full of soil and completely saturated, it was transferred to an oven set at 40 C to dry. This took approximately 24-48 hours. After the cores were completely dry, they were placed on top of an elevated mesh surface. 50 mL of the appropriate solution were added to the soil cores 6 times. The soil cores were allowed to completely dry between solution additions. This was approximately every 2 days. After the 6 solution injections, the soils were placed on top of a sand box. The water level was about 2 cm below the surface of the sand box and the soil cores were allowed to completely saturate. This saturation took approximately 2 days. Then the soil cores and materials were prepared for Typosoil™ measurements. After the Typosoil™ was done, the data was analyzed. The whole process took about two and a half weeks.

The two possible scenarios for CeO_2 addition were aqueous injection and mixing in to the soil. For the former scenario, the CeO_2 was prepared and added to the soil through the 50 mL solutions, added 6 times. For the latter scenario, the appropriate amount of CeO_2 was mixed into the soil before the soil cores were created in the metal cylinders (reconstition). Other than that, the two scenarios were treated the same.

3.2 Chemicals

CeO_2-NPs coated with polyvinylpyrrolidone (PVP) (20% wt/wt suspension, 30-50 nm) was purchased from the US Research Nanomaterials, Inc (Houston, TX). The nanoparticles have been characterized by Rossi, et. al. (2016) and the physicochemical properties of the nanoparticles are summarized below[1]: The CeO_2-NPs are primarily spherical with some polygonal nanoparticles, as shown by the Transmission Electron Microscopy (TEM) image in Figure 4. The size range is 20 – 110 nm with an average diameter of 55.6 nm. ImageJ (ver 1.46, National Institutes of Health, Bethesda, MD) was used to measure 270 NPs to acquire the size and size distribution data. The zeta potential, measured by a dynamic light scattering instrument (Zetasizer Nano ZS90, Malvern Instruments Ltd., Worcestershire, UK), was -51.8 mV for a 200 mg/L CeO_2-NPs solution (pH = 7). PVP-coated CeO_2 NPs were used because the PVP coating increases the stability of the NPs in solution. This PVP coating gives the NPs a negative surface charge, as shown by the zeta potential. NaCl was purchased from Fisher BioReagents.

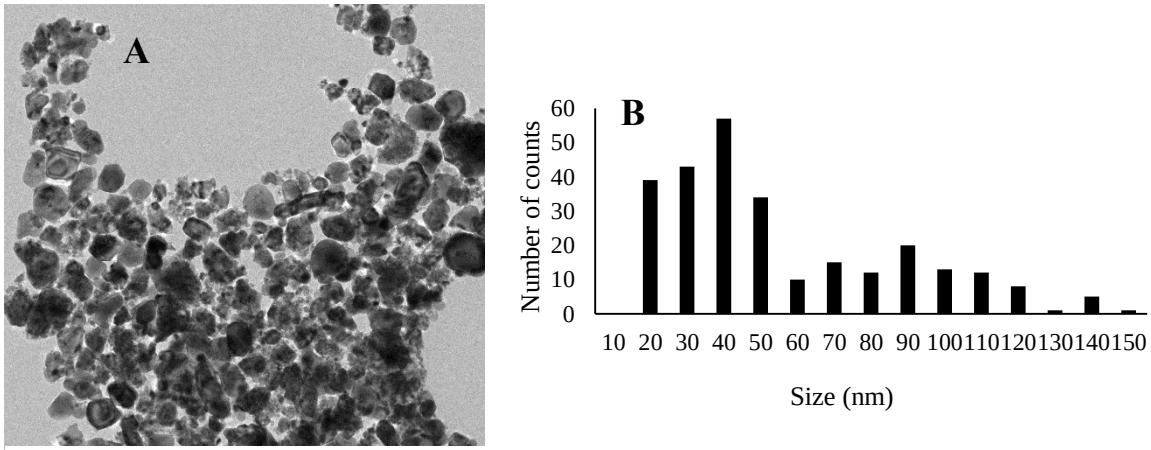

Figure 4: Transmission Electron Microscopy (TEM) imaging (A) and particle size distribution (B) of CeO_2 NPs. Reprinted from [1].

3.3 Soil Characterization

Soil collected from a residential lot in College Station, Texas was used for this study. Texas A&M Agrilife Extension performed a basic soil analysis to determine pH, conductivity, and elemental analysis. The results are summarized in Table 8. The particle size distribution is shown in Table 9. The soil is mostly silt (49.7%). Clay makes up 32.9% of the distribution, and sand is 17.4%. This soil is classified as a silty clay.

Table 8: Results of soil analysis performed by Texas A&M Agrilife Extention to find pH, conductivity, and elemental analysis

Analysis	Units	Replicate 1	Replicate 2	Replicate 3	Average
pH	-	8.1	8.1	8.1	8.1
Conductivity	umho/cm	266	272	279	272.33
Nitrate-N	mg/kg	0	0	0	0
Phosphorus	mg/kg	13	13	15	13.67
Potassium	mg/kg	166	149	169	161.33
Calcium	mg/kg	14229	13746	14966	14313.67
Magnesium	mg/kg	123	114	131	122.67
Sulfur	mg/kg	13	13	17	14.33
Sodium	mg/kg	8	8	8	8
Iron	mg/kg	6.96	7.36	7.6	7.31
Zinc	mg/kg	0.19	0.22	0.27	0.23
Manganese	mg/kg	4.39	4.42	5.41	4.74
Copper	mg/kg	0.24	0.26	0.28	0.26

Table 9: Particle size distribution of the College Station Residential Lot performed by the Texas A&M Agrilife Soil Characterization laboratory. The soil is 49.7% silt, 32.9% clay, and 17.4% sand.

PARTICLE SIZE DISTRIBUTION (mm)												
----------SAND----------						-------SILT-------		-------CLAY-------				
VC (2.0-1.0)	C (1.0-0.5)	M (0.5-0.25)	F (0.25-0.10)	VF (0.10-0.05)	TOTAL (2.0-0.05)	FINE (0.02-0.002)	TOTAL (0.05-0.002)	FINE (<0.0002)	TOTAL (<0.002)	TEXTURE CLASS	COARSE FRAG-MENTS %	ORGN C %
----------%----------												
1.6	2.9	3.4	3.7	5.8	17.4	32.1	49.7	4.1	32.9	SiCL		2.15

3.4 Experimental Setup

CeO_2-NPs were added to the soil by mimicking two scenarios of CeO_2-NPs introduction to soil: water irrigation and land biosolid disposal. Using biosolids could improve soil properties, like water holding capacity, and provide nutrients to the soil [48]. For the first method, CeO_2-NPs were prepared in an aqueous solution and injected into the soil. For the second method, CeO_2-NP dispersion and deionized water were added to the soil so that the soil reached full saturation and the target CeO_2 concentration. Detailed description on the introduction of CeO_2-NPs to soils are provided in the following sections (3.31 and 3.3.2). NaCl was added to the soil through application of a 50 mM aqueous solution. 50 mL of this solution was added to the soil a total of six times; this achieved a final soil concentration of 150 mmol NaCl/kg soil. There are six treatments for each method, as shown in Table 10 and Table 11. Each treatment had three replicates. The CeO_2 concentrations were chosen because these concentrations are frequently used in literature [1, 4, 5, 49]. The average salinity of saline soil and brackish water is 60 – 120 mM [1]. This NaCl concentration was chosen to imitate saline conditions, and this concentration has been used in previous literature [49, 50].

Table 10: Summary of the six soil treatments for scenario 1 – Injection. The solution concentration is the concentration of the solutions added to the soil. The final soil concentration are the concentrations of CeO_2-NP and NaCl after the injection of 50 mL of the aqueous solutions 6 times. The three CeO_2 concentrations are 0, 1500, and 6000 mg Ce/kg dry soil, and the two NaCl concentrations are 0 and 150 mmol NaCl/kg dry soil.

Injection Method			
Solution Concentration		**Final Soil Concentration**	
CeO_2 (mg/L)	**NaCl (mM)**	**Total CeO_2 (mg/kg)**	**Total NaCl (mmol/kg)**
0	0	0	0
500	0	1500	0
2000	0	6000	0
0	50	0	150
500	50	1500	150
2000	50	6000	150

Table 11: Summary of the 6 soil treatments for scenario 2 – mixing. NaCl is added through an aqueous solution (50 mM, 50 mL, 6 times). The three CeO_2 concentrations are 0, 500, and 2000 mg Ce/kg dry soil and the two NaCl concentrations are 0 and 150 mmol NaCl/kg dry soil.

Mixing Method		
Solution Concentration	**Final Soil Concentration**	
NaCl (mM)	**CeO_2 (mg/kg)**	**Total NaCl (mmol/kg)**
0	0	0
0	500	0
0	2000	0
50	0	150
50	500	150
50	2000	150

3.4.1 Application Method 1: Injection

In this application method, CeO_2-NPs are added to the soil through injection of an aqueous solution. The solutions were made as determined by treatment (Table 10). Enough CeO_2-NP suspension and/or NaCl was added to a volumetric flask to achieve the target concentration. 50 mL of the appropriate solution was added to the soil cores six times (see 3.5 Wetting and Drying Cycles). This gives the final soil concentration of CeO_2-NPs to be 0, 1500, and 6000 mg/kg_{soil} and the final NaCl concentrations to be 0 and 150 mmol/kg_{soil}.

3.4.2 Application Method 2: Mixed in

Water was added to 100 g of soil so that the soil was fully saturated (50 mL). CeO_2-NP dispersion and deionized water was added to soil at a proportion where the target CeO_2 concentration is achieved when the soil reached full saturation. Three CeO_2-NP concentrations were created: 0, 500, and 2000 mg/kg_{soil}. NaCl was added to deionized water to create the saline solution. The final concentrations of NaCl in soil were 0 and 150 mmol/kg_{soil}. In total, there were six treatments for this application method (Table 11).

3.5 Reconstitution

The soil was ground and sieved to 2 mm. A 5 cm height by 5 cm diameter metal cylinder was used to create the soil cores. A light layer of Vaseline was added to the inside of the cylinder to allow for easy removal of the soil later. The cylinder was placed on top of a filter paper in a shallow dish filled with water. Soil was then added to the cylinder in small increments, and the soil was allowed to become completely saturated with DI water before the next layer was added. Gentle tapping on the edge of the cylinder was performed in order to promote saturation. Soil was added evenly to the

cylinder to maintain a smooth surface throughout the process. Small amounts of soil were added evenly and allowed to saturate by capillary wetting to maintain the original soil structure as much as possible. Each core uses approximately 100 g of soil. Once the cylinder was filled with saturated soil, it was transferred to an oven to dry overnight at 40 °C. One core was created for each treatment. For application method 1 (injection), the same soil was used to create each of the 6 cores. For application method 2 (mixing), the specific mixed soil was used to create the 6 cores.

3.6 Wetting and Drying Cycles

Each soil core went through 6 wetting and drying cycles. 50 mL of the appropriate solution was added to the top of the soil core to fully saturate the soil, and the solution was allowed to percolate down the soil. Some leaching of the solution occurred out of the bottom of the soil core. Each core is approximately 100 g, and it was determined previously that 50 mL of water will fully saturate the soil. The soil was allowed to completely dry (approximately 2-3 days) between wetting cycles. This entire process took about 2 weeks.

3.7 Measuring Shrinkage Curve and Water Retention Curve

Once the wetting and drying cycles were completed, the soil cores were transferred to a sand box bath and removed from the metal cylinders. The water in the bath was maintained at a level 2 cm below the soil cores. The soil cores were left in the sand box bath for 1-2 days until they were fully saturated. Water was degassed by first boiling distilled water and then placing it under vacuum. The support platforms and tensiometers were flushed through with the degassed water until all air bubbles were removed. Then, the tensiometers were attached to the support platforms. The saturated soil cores were transferred to the support platforms, and the tensiometers were inserted

at half the height of the soil core to the depth where the tip of the tensiometer was approximately at the center of the soil core's diameter. A small spatula was used to smooth the soil around the tensiometer on the soil core to seal it in. The support platforms were placed in the TypoSoil™ at 40 °C until the mass of the soil cores stopped changing (approximately 2-3 days). This process was outlined in Assi et al (2014).

3.8 Determination of Hydro-Structural Parameters

The hydro-structural parameters were extracted from the best fit of the modeled shrinkage and water retention curve with raw measured data. The modeled shrinkage curve and water retention curve were created by using an optimization routine from Assi 2014 and Braudeau 2016 by minimizing the sum of squares between the modeled and measured shrinkage curve and water retention curve.

3.9 Statistical Analysis

Duncan's test for post hoc comparisons was performed at each CeO_2-NP concentration. One-way ANOVA was performed at each NaCl concentration. Two-way ANOVA was performed for all other parameters. The results are reported as mean ± standard error (n=3). All statistical tests were performed with IBM SPSS Statistics V22.0. Different letters and symbols in the figures represent significant differences among the treatments when the p-value was <0.05.

4. RESULTS AND DISCUSSION

4.1 CeO_2 Impact

There are two main soil-water characteristic curves to describe the soil medium: the water retention curve (WRC) and the shrinkage curve (ShC). The WRC is a measure of how much energy is required to remove water from the soil matrix. This is created by graphing the water suction (hPa) vs the specific water content (kg_{water}/kg_{soil}). The ShC is the specific volume of the soil (dm^3/kg_{soil}) vs the specific water content (kg_{water}/kg_{soil}). This describes the aggregate structure and water distribution within the pedostructure. There are three main characteristics that can be obtained from the WRC and the ShC: soil structure, potential energy of soil suction, and distribution of water among the macro- and micro-domains.

Figure 5 is the WRC (blue lines) and ShC (red lines) for each of the three CeO_2 concentrations (0, 1500, and 6000 mg CeO_2/kg_{soil}) without salt treatment. The first characteristic from the soil-water characteristic curves is the structure. This is obtained by examining the volume changes in the ShC. This characteristic was not studied in this experiment, but it is important to note that the CeO_2-NP either has no impact on the soil structure, or a slight positive affect at the 6000 CeO_2-NP concentration (figure 5).

The WRC demonstrates how much energy is required to remove water from the soil. The WRC begins at saturation and measures the soil suction with decreasing specific water content. Figure 5 shows that more potential is required to remove water from soil with increasing CeO_2 concentration. Figure 6 focuses on this trend. A vertical line is drawn at approximately 0.2 kg_{water}/kg_{soil}. At this water content, the 6000 mg/kg has the highest potential, followed by the 1500 mg/kg concentration, and the 0 mg/kg

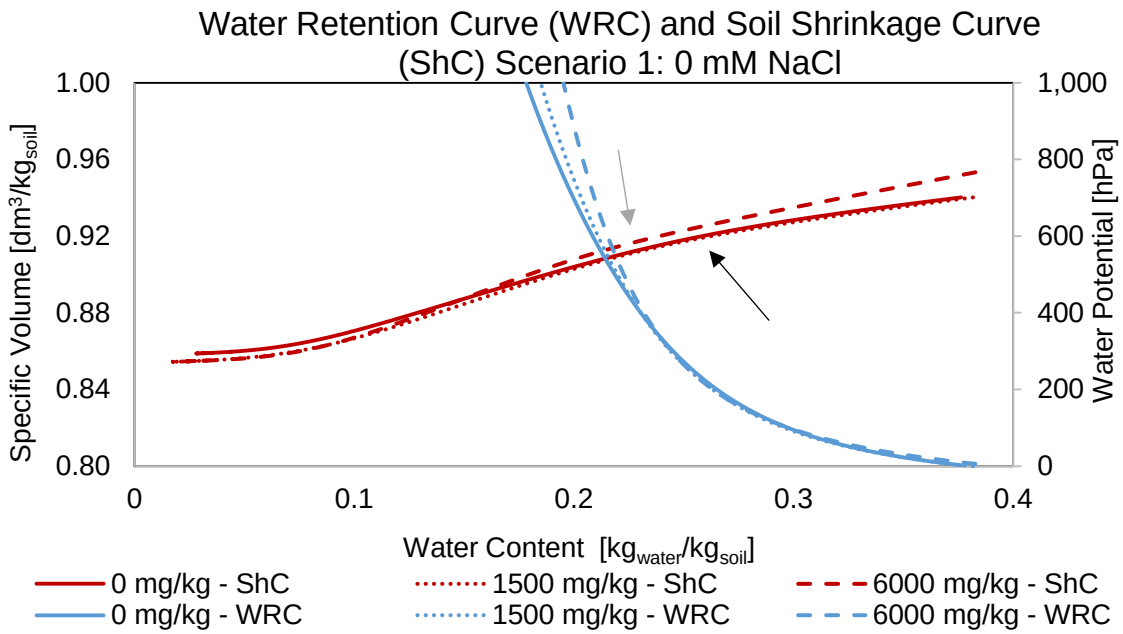

Figure 5: Water Retention Curve (WRC) and Soil Shrinkage Curve (ShC) for Scenario 1: Injection for the 3 CeO_2 concentrations at the 0 mM NaCl treatment

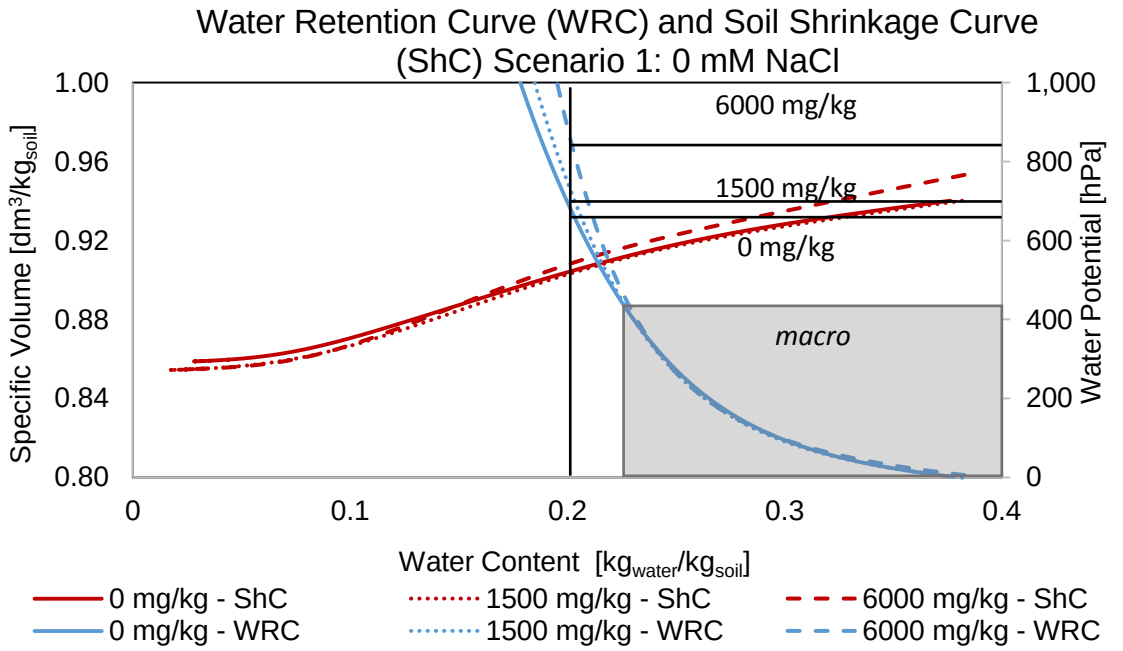

Figure 6: The water potential for each of the three CeO_2 concentrations for the 0 mM NaCl treatment of scenario 1 at water content of approximately 0.2 kg_{water}/kg_{soil}.

has the lowest potential. This indicates that in order to remove water from saturation to 0.2 kg_{water}/kg_{soil}, the 6000 mg/kg requires the most suction, or energy, to remove the same amount of water from the soil as the 0 and 1500 mg/kg concentrations. The gray box in figure 6 corresponds to the WRC of the macro water. This domain typically occurs in the region where the water potential is less than 400 hPa. The three CeO_2 concentrations have very similar curves in this region. The energy required from the macrodomain changes very little with CeO_2 concentration; the major change in the water potential occurs in the micro region.

The WRC is a measure of how tightly water is held by the soil, but it does not describe the water storage and distribution. These characteristics can be described by the ShC. Looking at the ShC for the 0 mM salt treatment in figure 6, the water distribution undergoes a slight change from the 0 and 1500 mg/kg CeO_2 treatments to the 6000 mg/kg. The 0 mg/kg and 1500 mg/kg treatments are almost identical. The transition point W_M, where the water content switches from the micro-pores to the macro-pores is around 0.25 kg water/kg soil. This is denoted by a black arrow in figure 5. This point is where the curve has a concave inflection point. This same transition point W_M (gray arrow) occurs at a lower water content for the 6000 mg/kg treatment, indicating that there is slightly more water present in the macropores at the 6000 mg/kg treatment than in the 0 and 1500 mg/kg treatment.

The WRC and ShC can provide a good foundation for understanding the soil-water characteristics, but it is important to be able to quantify this data. The hydro-structural parameters can be extracted from the modeled WRC and ShC to provide this information. There are 15 possible parameters, but this study will focus only on 5 to better understand the impact of CeO_2 on soil properties: E_{mi}, W_{sat}, W_{misat}, W_{masat}, and

W_{Nsat}. These 5 parameters are shown in Figure 7. W_{sat} is the water content at saturation, E_{mi} is the potential energy of the surface charge of the clay in the micropores, W_{misat} is the water content of the micropores at saturation. This corresponds to transition point W_M in the ShC, W_{masat} is the water content of the macropores at saturation, and W_{Nsat} is the dry water content of the primary peds. This is the residual water content.

Figure 7a .is the potential energy of the surface charge of the clay in the micropores. This is related to the WRC. Since the PVP coated CeO_2 NP are negatively charged, they can behave in the soil as the clay particles do. One theorized position for the CeO_2 NPs in the soil is on the outer edge of the primary peds in the microdomain but very close to the macropores. The addition of the negatively charged CeO_2 NPs to the primary peds increases the surface charge of the primary peds. This will also increase the potential energy inside the primary peds, as measured by E_{mi}. This trend is very clear and statistically significant: the CeO_2 NPs increase the potential energy of the surface charge of the clay particles inside the primary peds. This is supported by the trends seen in the WRC. A higher E_{mi} means that more energy is required to remove water from the microdomain.

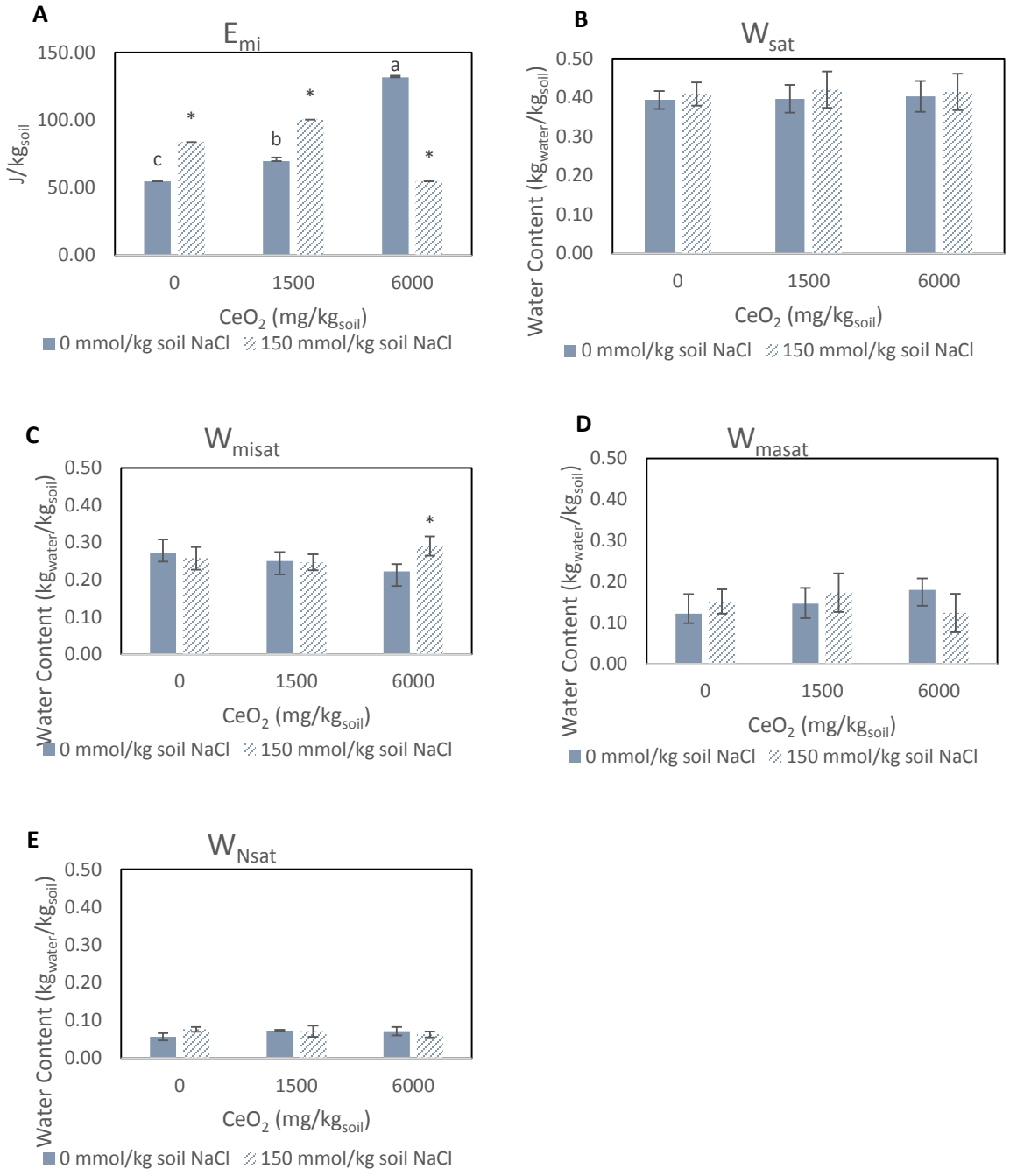

*Figure 7: The hydro-structural parameters extracted from the modeled ShC and WRC for scenario 1. (A) E_{mi} is the potential energy of the surface charge of the clay in the micropores, (B) W_{sat} is the water content at saturation, (C) W_{misat} is the water content of the micropores at saturation. This corresponds to transition point W_M in the ShC, (D) W_{masat} is the water content of the macropores at saturation. W_{misat} and W_{masat} equal W_{sat}, (E) W_{Nsat} is the dry water content of the primary peds. This is the residual water. The different letters indicate a statistically significant difference between CeO_2 concentrations across the 0 mM salt treatment. The asterisk * indicates a statistically significant difference between the 2 salt treatments at the same CeO_2 concentration.*

Figures 7b-e examine the water storage and distribution within the soil sample. Figure 7b shows that there is no large differences in W_{sat}, indicating that there is no overall change in the water content of the soil at saturation. W_{misat} and W_{masat} are the water contents of the soil sample in the microdomain and macrodomain, respectively. These two parameters will describe the distribution of water within the soil. There is no statistically significant changes here, but there are some observations of the trends. As CeO_2 concentration increases, there is a very small increase in W_{Nsat}. Even though it is not significant, there is also an increase in W_{masat} and a decrease in W_{misat} with increasing CeO_2 NP concentration. This means that there could be a slight shift in the water distribution in favor of the macrodomain with the addition of CeO_2 NPs.

This observation could be explained by the increase in E_{mi}. An increase in surface potential typically increases the double layer. Within the primary peds, the increase in E_{mi} could cause a small increase in the double layer thickness, causing the particles to be pushed apart slightly. As demonstrated previously, an increase in the double layer thickness usually leads to a higher water retention. Therefore, the water content of the primary peds at the air entry point could be slightly higher when the CeO_2 concentration is increased. This would be demonstrated by an increase in W_{Nsat} and a decrease in W_{misat}. According to eqution [10], $W_{sat} = W_{misat} + W_{masat}$, so a decrease in W_{misat} would correspond to a slight shift of the water content to the macrodomain.

A second explanation is that the position of the CeO_2 NPs is on the edge of the primary peds, close enough to interact with the macrodomain. Similar to the surface potential increase within the primary ped, there could be a small increase in the surface potential outside the primary ped (E_{ma}). The same behavior would follow: an increase in

the E_{ma} leads to an increase in the double layer thickness, so more water is retained in the macropores.

4.2 NaCl Treatment the Intersection of CeO_2 and NaCl

All of the previous data and observations were made for the 0 mM NaCl treatment. Figure 8 shows the WRC and ShC for the 50 mM NaCl salt treatment. There is no linear trend for either curve. The change in WRC is not as pronounced for the 50 mM NaCl salt treatment as for the 0 mM treatment. Additionally, the most energy is required to remove water from the 1500 mg/kg CeO_2 concentration, followed by the 0 mg/kg concentration, and the 6000 mg/kg concentration requires the least amount of energy (figure 9). On the ShC (red line), it is very difficult to discern the transition point W_M, but it appears that the 6000 mg/kg CeO_2 treatment has the smallest macrodomain. This is shown by the black arrow for the 0 and 1500 mg/kg CeO_2 concentrations and the gray arrow for the 6000 mg/kg CeO_2 concentration in figure 8. The hydro-structural parameters in figure 7 also do not follow a clear pattern. Even though there are some significant differences, no conclusions can be drawn. When the 50 mM NaCl solution was added to the soil during the wetting and drying cycles, the cores were placed on a wire mesh surface. Therefore, solution was allowed to leach out of the soil. It is possible that some of the NaCl was leached out of the soil. It is also possible that Na^+ was replacing other cations in the soil, such as Ca^{2+} and Mg^{2+}. In this case, the NaCl is not increasing the total salinity concentration in the soil, it is only increasing the exchangeable sodium percentage. This will increase the sodicity of the soil rather than the salinity. There also may be some counteracting forces at work with respect to the double layer. Increasing the valence of the cations on the double layer will decrease the thickness when all other factors remain constant. Increasing the ionic strength of the

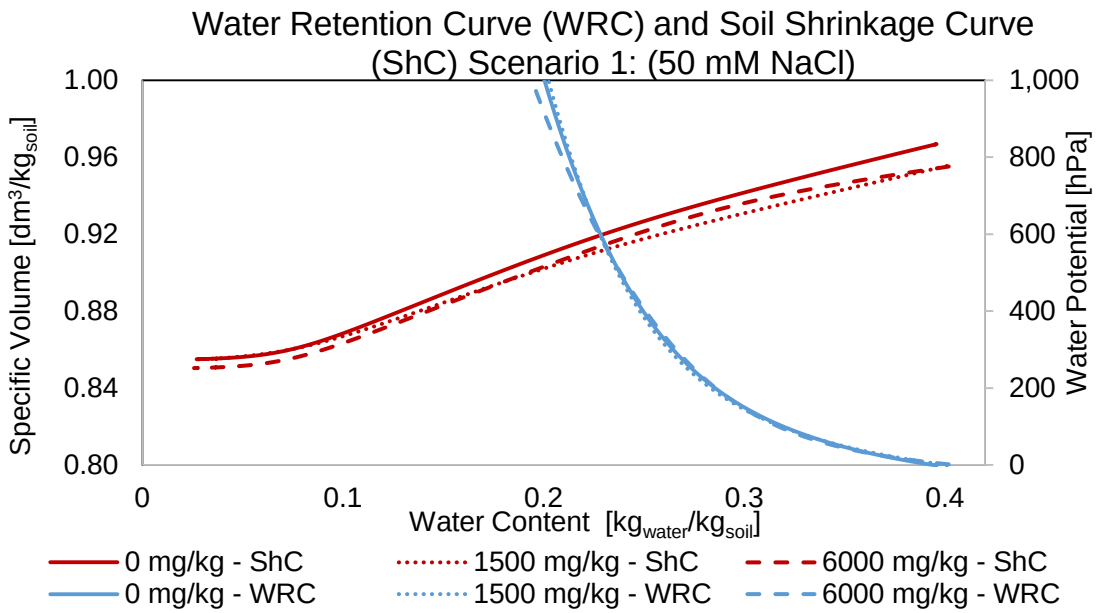

Figure 8: Water Retention Curve (WRC) and Soil Shrinkage Curve (ShC) for Scenario 1: Injection for the 3 CeO_2 concentrations at the 50 mM NaCl treatment

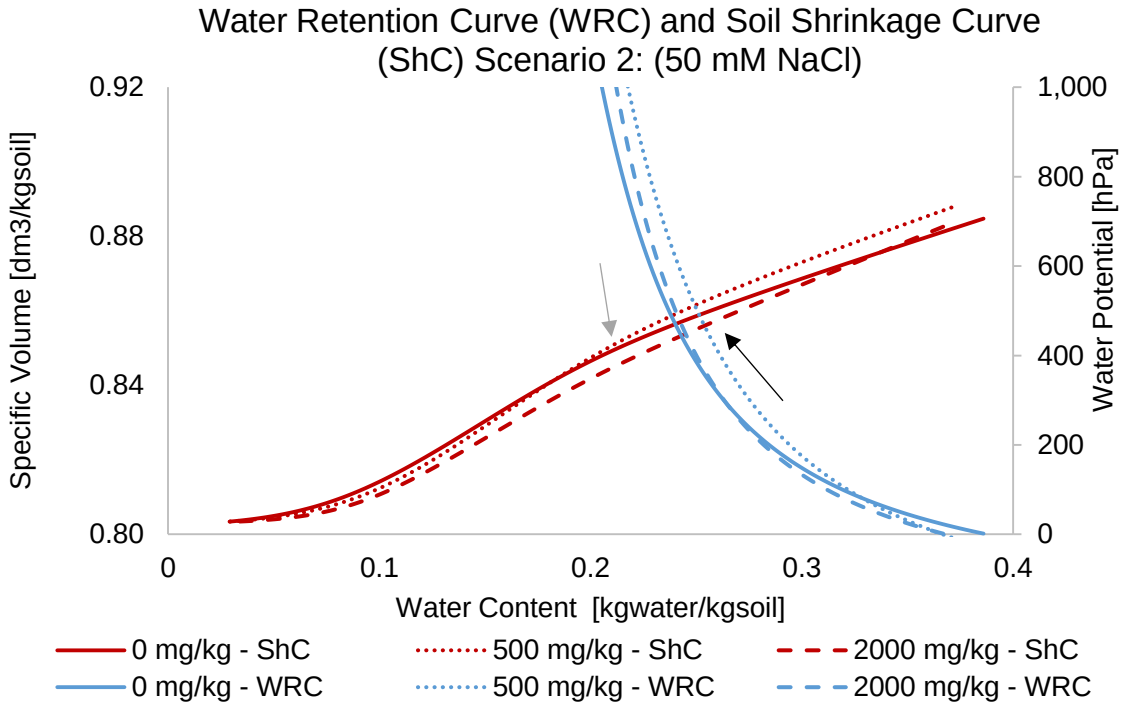

Figure 9: Water Retention Curve (WRC) and Soil Shrinkage Curve (ShC) for Scenario 2: Mixing for the 3 CeO_2 concentrations at the 50 mM NaCl treatment

solution will also decrease the thickness of the double layer. Increasing the NaCl concentration will decrease the valence of the cations and increase the ionic strength. The first will increase the double layer thickness, while the second will decrease it. This could be an explanation for why the hydrostructural properties in figure 7 do not follow a linear trend. Figure 9 shows the WRC and ShC curves for scenario 2: mixing for the three CeO_2 concentrations at the 50 mM salt treatment, and figure 11 shows the hydrostructural parameters. This data is also inconclusive for the same reasons as scenario 1. Further investigation is required to describe the impact of NaCl and CeO_2 on the soil properties.

4.3 Application Methods

The scenarios are not at the same CeO_2 concentrations, so they cannot be compared directly. But the general trends can be compared. The results for scenario 2 are very similar to the results for scenario 1. For the 0 mM NaCl treatment, more energy is required to remove water from the soil as the CeO_2 concentration increases (figure 10). This is further demonstrated in figure 11. A vertical line is drawn at approximately 0.22 kg_{water}/kg_{soil}. The 2000 mg/kg CeO_2 concentration has the highest potential at this water content, so it requires the most energy to remove water. The 500 mg/kg CeO_2 has the next highest potential, and the 0 mg/kg concentration has the lowest potential. This follows the same trends as seen in figures 5 and 6 for scenario 1. However, the difference between the highest CeO_2 potential and the lowest is much larger than in scenario 1. Additionally, figure 10 shows that there is some difference in the water potential of the macroregion of scenario 2. The difference in the water potential is supported by the increase in E_{mi} with increasing CeO_2 concentration (figure 10).

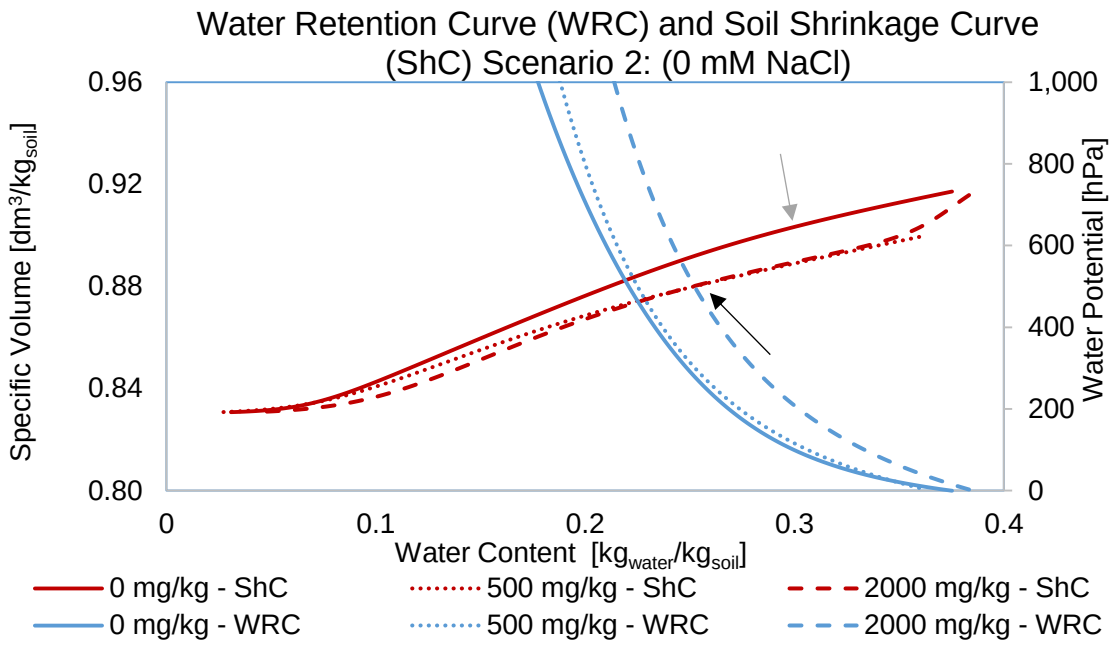

Figure 10: Water Retention Curve (WRC) and Soil Shrinkage Curve (ShC) for Scenario 2: Mixing for the 3 CeO_2 concentrations at the 0 mM NaCl treatment

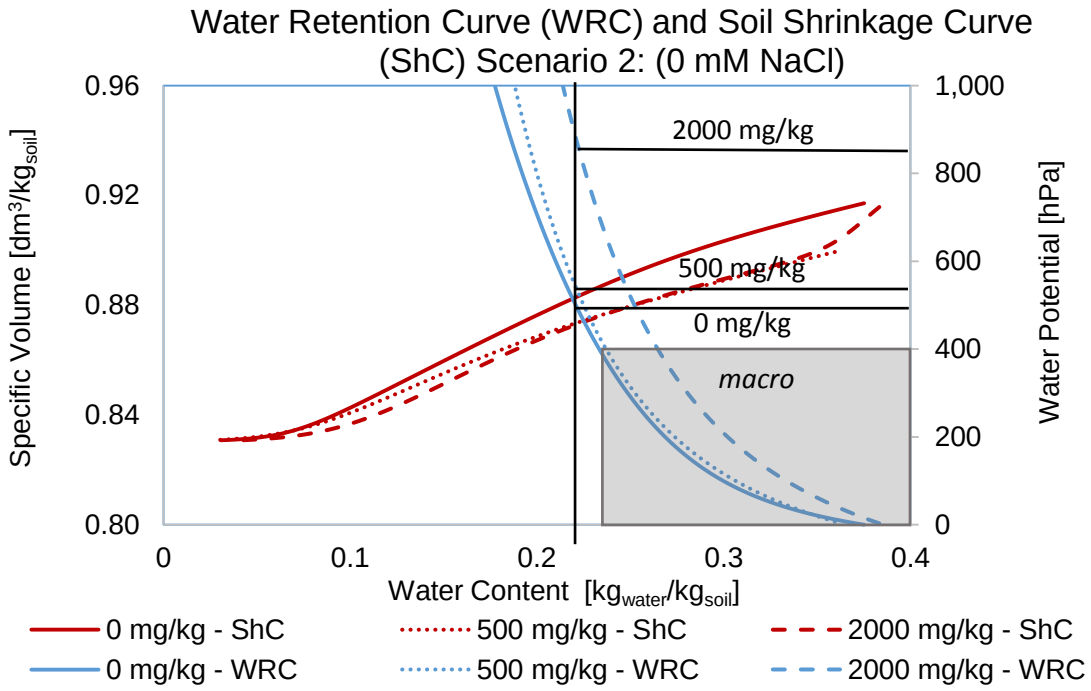

Figure 11: A water content of approximately 0.18 kg_{water}/kg_{soil} was chosen to demonstrate the water potential of each of the three CeO_2 concentrations for the 0 mM NaCl treatment.

The ShC curve in figure 10 shows that there may be a shift towards the macroregion with increasing CeO_2 concentration. The 500 and 2000 mg/kg concentrations have very similar ShC, and the transition point W_M occurs at a lower water content than for the 0 mg/kg concentration. The gray arrow is W_M for the 0 mg/kg concentration (water content of approximately 0.30), and the black arrow shows W_M for the 500 and 2000 mg/kg CeO_2 concentrations (approximately 0.24). This means that more water is present in the macroregion at higher CeO_2 concentrations. This observation, while not statistically significant, can be seen in the W_{misat} and W_{masat} parameters. Figure 12 shows that there is no overall change in the W_{sat}, so the water storage capacity of the soil isn't changing. There is a very small increase in W_N at the 2000 mg/kg concentration as compared to the 0 and 500 mg/kg concentrations. There is also a small decrease in W_{misat} and a small increase in W_{masat}. These observations were also seen in scenario 1. This supports the hypothesis that the application methods will have similar trends

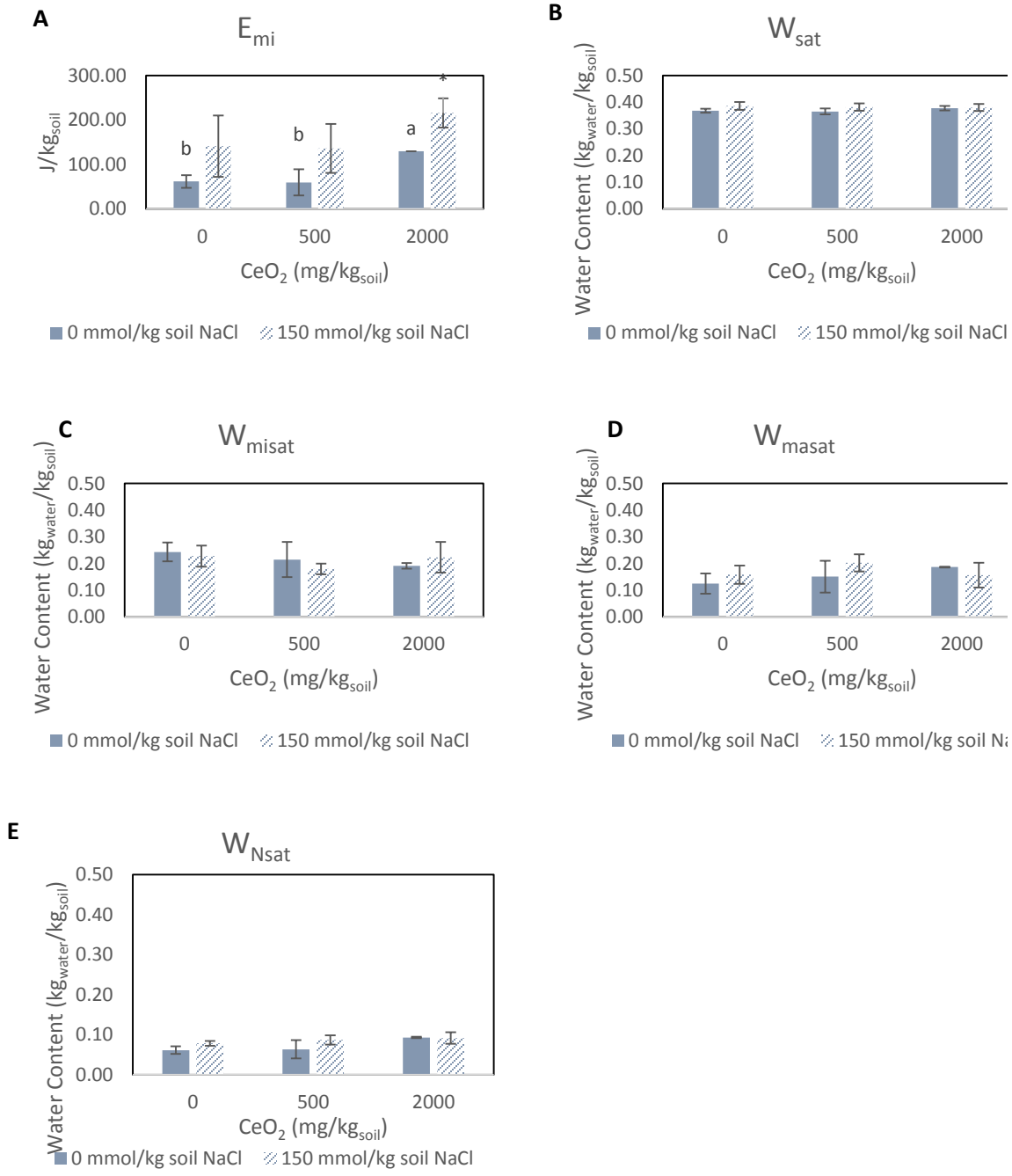

*Figure 12: The extracted hydro-structural parameters from the ShC and WRC for scenario 2. (A) E_{mi} is the potential energy of the surface charge of the clay in the micropores, (B) W_{sat} is the water content at saturation, (C) W_{misat} is the water content of the micropores at saturation. This corresponds to transition point W_M in the ShC, (D) W_{masat} is the water content of the macropores at saturation. W_{misat} and W_{masat} equal W_{sat}, (E) W_{Nsat} is the dry water content of the primary peds. This is the residual water. The different letters indicate a statistically significant difference between CeO_2 concentrations across the 0 mM salt treatment. The asterisk * indicates a statistically significant difference between the 2 salt treatments at the same CeO_2 concentration*.

5. SUMMARY

5.1 Conclusions

The data was inconclusive for the 50 mM NaCl treatments. Further experimentation is required to determine the impact of NaCl and CeO_2 NP interaction on soil-water properties. The two scenarios cannot be directly compared, but there are some interesting patterns and observations in the 0 mM NaCl treatment for both application scenarios. It is very clear that increasing the CeO_2-NP concentration corresponds to an increase in the E_{mi} parameter, or the potential energy of the surface charge of the clay particles inside the micropores. This demonstrates an increase in surface charge. PVP-coated CeO_2 NPs are negatively charged, so when they are introduced into the soil environment, they can act as clay particles do, artificially creating a more clayey soil. A second trend was no change in W_{sat}, a slight increase in the W_{masat} and slight decrease in the W_{misat}. Although this wasn't statistically significant, this observation was present in both the ShC and hydro-structural parameters. This indicates that although CeO_2-NP doesn't change the total water holding capacity, it may affect the distribution of water by moving water from the micropores to the macropores.

These results together have some interesting insinuations for plants. The increase in water potential indicates that it is harder for water to be removed from the micropores at higher CeO_2 concentrations. However, there may be a shift in the water distribution towards the macropores, where it is easier for plants to remove water. These slightly contradictory implications match up with the same contradictory results found in the studies of CeO_2 on plants, as demonstrated in section 2.1. However, this information of the water distribution can be used for soil-water management strategies

to know what crops to grow and how many, and when and how much to irrigate. Extending this research into different soil types will add to the soil-water management strategies. Since the CeO_2 NPs appear to increase the clayey behavior of a soil, it could be used on sandy soil to improve water retention. This type of soil could then be used for agriculture, where it was difficult before. Overall, the results of this study demonstrate that the CeO2 nanoparticles do have an effect on soil properties.

5.2 Recommendations for Future Work

This study laid the groundwork for future studies regarding the impact of CeO_2 NPs on soil-water properties. In this study, the experiments involving NaCl were inconclusive. In future works, it would be prudent to remove the NaCl component and simply focus on the impact of the nanoparticles. An extension of this study would be to determine the exact amount of surface charge on the clay particles and the amount of surface charge added by the CeO_2 NPs. This could be done through the determination of the CEC of the soil and calculations from the concentration and zeta potential of the CeO_2 NPs. The first of future studies could be to change the soil type. Since it is hypothesized that the majority of the CeO_2 interaction with the soil occurred with the clay particles, the soil type could play a major role in how the CeO_2 NPs interact with the soil. If a sandy soil was used, after introducing NPs into the soil environment, it is expected that the soil would have more clayey characteristics, including increased water retention. This would be useful for agriculture because then plants could be grown in more areas.

One of the more unique properties of CeO_2 NPs is their UV radiation absorption capabilities. One possible experiment would be to treat one set of CeO_2 treated soil cores with UV light and compare the soil-water properties to a control. Although very

few differences between the control and the UV-irradiated samples would be expected since there is no change to the NP structure, especially in the field where very little sunlight would penetrate the soil to the depth where the roots extract water from the soil, this would be an interesting dimension to the impact of CeO_2 NPs on soil.

The CeO_2 NPs used in this study were coated with PVP, which gave them a negative charge. Non-coated CeO_2 NPs would have a positive charge. It is hypothesized that these nanoparticles would still interact with the clay particles, but in this case, they would have opposite charges. This would directly impact the surface potential with an expected decrease.

Furthermore, it is important to test different types of nanoparticles, such as TiO_2 or SiO_2, which could be introduced into soil environments. There could be very few differences from the impact of CeO_2 NPs since the interaction with the clay particles comes from size and charge, but there could also be other interactions based on the unique properties of each nanoparticle.

This study used 6 wetting and drying cycles to represent approximately a 2 week irrigation cycle. Another study would be to adjust the number of wetting and drying cycles to determine if the length of interaction between soil and nanoparticles is a factor in the impact on the soil-water characteristics.

Implications for plant growth can be made based on the results of the impact of the ENPs on soil-water properties. But an extra aspect would be to simultaneously grow plants in identical conditions to the soil cores being tested by the Typosoil to directly compare the results. This study could be done with a variety of plants, ENPs, and soil types.

Finally, after all the aspects of the impacts of solely nanoparticles on soil have been studies, NaCl should be reintroduced. In order to more accurately examine the impact of the intersection of NaCl and ENPs on the soil properties, the CEC should be measured before and after the addition of NaCl and the ENPs. The EC should also be measured along with pH to determine how much NaCl is being added to the soil, and what the exchangeable sodium percentage is, and how the NaCl is interacting with the soil. It is expected that the impact of the interaction between ENPS and NaCl will change based on the concentration of each input, so a variety of concentrations should be tested.

The results of this study are only the beginning of understanding the impact of CeO_2 NPs on soil-water properties. There are several directions to go in order to more fully comprehend the entirety of this study.

REFERENCES

1. Rossi, L., et al., *The impact of cerium oxide nanoparticles on the salt stress responses of Brassica napus L.* Environmental Pollutution, 2016. **219**: p. 28-36.
2. Ma, X., et al., *Interactions between engineered nanoparticles (ENPs) and plants: phytotoxicity, uptake and accumulation.* Science of the Total Environment, 2010. **408**(16): p. 3053-61.
3. Nel, A., *Toxic Potential of Materials at the Nanolevel.* Science, 2006. **311**(5761): p. 622-627.
4. Lopez-Moreno, M.L., et al., *X-ray absorption spectroscopy (XAS) corroboration of the uptake and storage of CeO(2) nanoparticles and assessment of their differential toxicity in four edible plant species.* Journal of Agricultural and Food Chemistry, 2010. **58**(6): p. 3689-93.
5. Ma, Y., et al., *Origin of the different phytotoxicity and biotransformation of cerium and lanthanum oxide nanoparticles in cucumber.* Nanotoxicology, 2015. **9**(2): p. 262-70.
6. Ma, X., et al., *Multigenerational exposure to cerium oxide nanoparticles: Physiological and biochemical analysis reveals transmissible changes in rapid cycling Brassica rapa.* NanoImpact, 2016. **1**: p. 46-54.
7. Roco, M.C., *The long view of nanotechnology development: the National Nanotechnology Initiative at 10 years.* Journal of Nanoparticle Research, 2011. **13**(2): p. 427-445.

8. Franklin, N.M., et al., *Comparative Toxicity of Nanoparticulate ZnO, Bulk ZnO, and ZnCl2to a Freshwater Microalga (Pseudokirchneriella subcapitata): The Importance of Particle Solubility.* Environmental Science & Technology, 2007. **41**(24): p. 8484-8490.

9. Wang, Q., et al., *The impact of cerium oxide nanoparticles on tomato (Solanum lycopersicum L.) and its implications for food safety.* Metallomics, 2012. **4**(10): p. 1105-12.

10. Qadir, M., et al., *Non-conventional water resources and opportunities for water augmentation to achieve food security in water scarce countries.* Agricultural Water Management, 2007. **87**(1): p. 2-22.

11. Munns, R. and M. Tester, *Mechanisms of salinity tolerance.* Annual Review of Plant Biology, 2008. **59**: p. 651-81.

12. Rengasamy, P., *Soil processes affecting crop production in salt-affected soils.* Functional Plant Biology, 2010. **37**(7): p. 613.

13. FAO. *FAO Land and Plant Nutrition Management Service*. [Web] 2008 [cited 2017]; Available from: http://www.fao.org/ag/agl/agll/spush

14. Zaghdoud, C., et al., *Health-promoting compounds of broccoli (Brassica oleracea L. var. italica) plants as affected by nitrogen fertilisation in projected future climatic change environments.* Journal of the Science of Food and Agriculture, 2016. **96**(2): p. 392-403.

15. López-Moreno, M.L., et al., *Evidence of the Differential Biotransformation and Genotoxicity of ZnO and CeO2Nanoparticles on Soybean (Glycine max) Plants.* Environmental Science & Technology, 2010. **44**(19): p. 7315-7320.

16. Ma, X., et al., *Cerium Oxide Nanoparticles and Bulk Cerium Oxide Leading to Different Physiological and Biochemical Responses in Brassica rapa.* Environmental Science & Technology, 2016. **50**(13): p. 6793-802.

17. Zhao, L., et al., *CeO2and ZnO Nanoparticles Change the Nutritional Qualities of Cucumber (Cucumis sativus).* Journal of Agricultural and Food Chemistry, 2014. **62**(13): p. 2752-2759.

18. Yaron, B., I. Dror, and B. Berkowitz, *Engineered nanomaterials as a potential metapedogenetic factor: A perspective.* Catena, 2016. **146**: p. 30-37.

19. Westerhoff, P. and B. Nowack, *Searching for Global Descriptors of Engineered Nanomaterial Fate and Transport in the Environment.* Accounts of Chemical Research, 2013. **46**(3): p. 844-853.

20. Mogyorósi, K., I. Dékány, and J.H. Fendler, *Preparation and Characterization of Clay Mineral Intercalated Titanium Dioxide Nanoparticles.* Langmuir, 2003. **19**(7): p. 2938-2946.

21. Zhou, D., A.I. Abdel-Fattah, and A.A. Keller, *Clay Particles Destabilize Engineered Nanoparticles in Aqueous Environments.* Environmental Science & Technology, 2012. **46**(14): p. 7520-7526.

22. Ben-Moshe, T., et al., *Effects of metal oxide nanoparticles on soil properties.* Chemosphere, 2013. **90**(2): p. 640-646.

23. Wang, D., et al., *Hyperexponential and nonmonotonic retention of polyvinylpyrrolidone-coated silver nanoparticles in an Ultisol.* Journal of Contaminant Hydrology, 2014. **164**: p. 35-48.

24. Cornelis, G., et al., *Fate and Bioavailability of Engineered Nanoparticles in Soils: A Review.* Critical Reviews in Environmental Science and Technology, 2014. **44**(24): p. 2720-2764.

25. Ng, C.W.W. and J.L. Coo, *Hydraulic conductivity of clay mixed with nanomaterials.* Canadian Geotechnical Journal, 2015. **52**(6): p. 808-811.

26. Tellam, J., et al. *Manufactured nanoparticle movement in the groundwaters of a redbed sandstone: laboratory experiments and field observations*. in *GQ10: Groundwater Quality Management in a Rapidly Changing World*. 2010. Zurich, Switzerland: IAHS.

27. Dunphy Guzman, K.A., M.P. Finnegan, and J.F. Banfield, *Influence of Surface Potential on Aggregation and Transport of Titania Nanoparticles.* Environmental Science & Technology, 2006. **40**(24): p. 7688-7693.

28. Singh, A., *Integrated Water Management: Water and Plant Growth.* 2007: p. 1-16.

29. Olorunfemi, I., J. Fasinmirin, and A. Ojo, *Modeling cation exchange capacity and soil water holding capacity from basic soil properties.* Eurasian Journal of Soil Science, 2016. **5**(4): p. 266.

30. Horne, D.J. and D.R. Scotter, *The available water holding capacity of soils under pasture.* Agricultural Water Management, 2016. **177**: p. 165-171.

31. R., V. and P.P. Rajesh, *Assessment of Water Holding Capacity of Major Soil Series of Lalgudi, Trichy, India.* Journal of Environmental Research And Development, 2012. **7**(1A): p. 393-398.

32. Senjobi, B.A. and O.A. Ogunkunle, *Effect of Land Use on Soil Degradation and Soil Productivity Decline on Alfisols and Ultisols in Ogun State in South Western, Nigeria.* Agriculturae Conspectus Scientificus, 2010. **75**(1): p. 9-19.

33. Reynolds, C.A., T.J. Jackson, and W.J. Rawls, *Estimating soil water-holding capacities by linking the Food and Agriculture Organization Soil map of the world with global pedon databases and continuous pedotransfer functions.* Water Resources Research, 2000. **36**(12): p. 3653-3662.

34. Assi, A.T., et al., *Physics of the soil medium organization part 2: pedostructure characterization through measurement and modeling of the soil moisture characteristic curves.* Frontiers in Environmental Science, 2014. **2**: p. 1-17.

35. Braudeau, E., et al., *Physics of the soil medium organization part 1: thermodynamic formulation of the pedostructure water retention and shrinkage curves.* Frontiers in Environmental Science, 2014. **2**: p. 1-17.

36. Braudeau, E.F. and R.H. Mohtar, *A framework for soil-water modeling using the pedostructure and Structural Representative Elementary Volume (SREV) concepts.* Frontiers in Environmental Science, 2014. **2**: p. 1-13.

37. Braudeau, E., et al., *Soil water thermodynamic to unify water retention curve by pressure plates and tensiometer.* Frontiers in Earth Science, 2014. **2**: p. 1-13.

38. Braudeau, E., *Hydrostructural pedology*. 2016, Hoboken, NJ: ISTE Ltd/John Wiley and Sons Inc. pages cm.

39. Meade, R.H., *Fabric and Mineral Analysis of Soils. Roy Brewer. Wiley, New York, 1964. xiv + 470 pp. Illus. $15.* Science, 1965. **148**(3668): p. 355-356.

40. Braudeau, E. and R. Mohtar, *Encyclopedia of Agricultural, Food, and Biological Engineering*, in *Integrative Environmental Modeling*, D. Heldman and C. Moraru, Editors. 2010, Taylor & Francis: New York. p. 1-6.

41. Yong, R.N., M. Nakano, and R. Pusch, *Environmental soil properties and behaviour*. 2012, Boca Raton, FL: CRC Press. xix, 435 p.

42. Fedkin, M., et al., *Understanding the Water Retention of Composite Proton Exchange Membranes Based on Surface Chemistry of Inorganic Fillers.* ECS Transactions, 2008. **11**: p. 189-198.

43. Tuller, M. and D. Or, *Water films and scaling of soil characteristic curves at low water contents.* Water Resources Research, 2005. **41**(9).

44. Sparks, D.L., *Soil physical chemistry*. 2nd ed. 1999, Boca Raton, Fla.: CRC Press. 409 p.

45. Yong, R.N., *Geoenvironmental engineering : contaminated soils, pollutant fate and mitigation*. 2001, Boca Raton, Fla.: CRC Press. 307 p.

46. François, B. and S. Ettahiri. *Role of the Soil Mineralogy on the Temperature Dependence of the Water Retention Curve*. in *Second European Conference on Unsaturated Soils, E-UNSAT 2012*. 2012. Napoli, Italy: Springer-Verlag Berlin Heidelberg.

47. El-Swaify, S.A. and D.W. Henderson, *Water Retention by Osmotic Swelling of Certain Colloidal Clays with Varying Ionic Composition.* Journal of Soil Science, 1967. **18**(2): p. 223-232.

48. *Biosolids Technology Factsheet: Land Application of Biosolids*, in *Office of Water*, M.T. Branch, Editor. September 2000, Environmental Protection Agency: Washington, D.C.

49. Ma, Y., et al., *Effects of rare earth oxide nanoparticles on root elongation of plants.* Chemosphere, 2010. **78**(3): p. 273-279.

50. Yousuf, P.Y., et al., *Salt stress-induced modulations in the shoot proteome of Brassica juncea genotypes.* Environmental Science and Pollution Research, 2015. **23**(3): p. 2391-2401.